



## Article

# Analysis and Design of a Minimalist Step Climbing Robot

Nayan Jyoti Baishya <sup>1,\*</sup> , Bishakh Bhattacharya <sup>2</sup> , Harutoshi Ogai <sup>1</sup> and Kohei Tatsumi <sup>1</sup>

<sup>1</sup> Graduate School of Information, Production and Systems (IPS), Waseda University, 2-7 Hibikino, Fukuoka 808-0135, Japan; ogai@waseda.jp (H.O.); tatsumi.kohei@waseda.jp (K.T.)

<sup>2</sup> Indian Institute of Technology Kanpur, Kanpur 208016, India; bishakh@iitk.ac.in

\* Correspondence: nayanb@fuji.waseda.jp

**Abstract:** In this article, a novel yet simple step climbing robot is proposed and is comprised of two front wheels, a rear-wheel and an actuator to vary the center distance between the front and rear wheels. When a robot climbs a stair, the huge variance in the inclination angle of the robot may result in its toppling. Hence, a mechanism is proposed to compensate for the change in inclination angle. An inertial measuring unit (IMU) is used to sense the inclination angle of the robot which is then fed to a microcontroller in order to actuate the connecting link, thereby reducing the variation of the inclination angle. During ascending simulations on dynamic model based on the Newton–Euler formulation, the required torque on rear wheel is reduced by 26.3% as compared to uncontrolled simulations. Moreover, the normal reaction on rear wheel during descending simulation has increased by 170.9% by controlling the inclination angle, which reduced the probability of toppling of the proposed robot. Multiple experiments on the prototype with a controlled condition show that the variation in inclination angle is reduced by 77.8% during ascending, whereas it is reduced by 92.8% during descending resulting in successful operation on the stairs as compared to uncontrolled cases.

**Keywords:** stair climbing robot; three-wheel robot; wheeled mobile robot (WMR); assistive robot; assistive technologies; power assist; kinematics; dynamic model



**Citation:** Baishya, N.J.; Bhattacharya, B.; Ogai, H.; Tatsumi, K. Analysis and Design of a Minimalist Step Climbing Robot. *Appl. Sci.* **2021**, *11*, 7044. <https://doi.org/10.3390/app11157044>

Academic Editors: Adel Razek and Alberto Doria

Received: 11 May 2021

Accepted: 27 July 2021

Published: 30 July 2021

**Publisher's Note:** MDPI stays neutral with regard to jurisdictional claims in published maps and institutional affiliations.



**Copyright:** © 2021 by the authors. Licensee MDPI, Basel, Switzerland. This article is an open access article distributed under the terms and conditions of the Creative Commons Attribution (CC BY) license (<https://creativecommons.org/licenses/by/4.0/>).

## 1. Introduction

In the past few decades, enormous development in the field of robotics has resulted in replacing human tasks with robots. Similar advancement of technologies has also been observed in the development of delivery robots, such as packaging robots, autonomous driving robots, etc. One of the major aspects of today's delivery system comprises door-to-door delivery. In order to achieve complete autonomy in such delivery systems, a robot must be capable of climbing the stairs (up and down) of a building.

Extensive research has been undertaken by many researchers to develop robots with climbing capabilities. These robots are broadly categorized into three groups: tracked, articulated leg and hybrid system. In a track based stair climbing system [1], track belts are used to drive the robot. Lawn et al. proposed to replace single track belt system with a set of two track-belt system to improve the stability of a step climbing wheelchair [2]. Research was conducted to develop a novel variable geometry tracked mechanism [3]. Such systems are highly controllable and can successfully maneuver on rough terrains and stairs. However, these systems are slower as compared to the wheel based systems. On the other hand, systems based on articulate legs [4] are highly effective in climbing stairs, although they are quite complex to control. Hence, many researchers tend to work towards the development of hybrid systems, which can be further classified into two categories: wheels with track [5] and wheels with articulated legs [6]. A hybrid shrimp mechanism consisting a front fork, a body and a parallel bogies was developed to maneuver in an unstructured environment for rescue operations [7]. Woo et al. proposed a step climbing robot based on passive four bar linkage type locomotive motion [8]. In an another hybrid mechanism, the use of two legs with seven degrees of freedom is discussed [9]. In an interesting

research study, a eight legged (four pair) hybrid step climbing robot was proposed. The step climbing is achieved by controlling the height of each pair of the legs [10]. Zuniga et al. illustrated a novel step climbing robot consisting a pair of rotating links at the front and back of the robot [11]. A hybrid leg-wheel robot termed as the Mantis robot was developed and the front links were used as clamps and pulled the main body of robot to overcome any obstacle [12]. A novel step climbing robot consisting two pairs of half circled legs is proposed by Qiao et al. [13]. In yet another case, a separate attachable stair climbing module has been developed, which can be attached or detached based on the requirement [14]. The attached module consists of linear actuators that pushes the robot in an upward direction. Although this system is lightweight, it requires human assistance.

In [15], powered linkage-based mechanisms along with clustered wheels for the purpose of achieving high step climbing capabilities have been proposed. While powered links help in pushing the robot, clustered wheels take care of obstacle avoidance. In another research study, a swing arm based linkage mechanism was proposed [16]. Another interesting group of hybrid systems are available in the open literature [17–22], presented by Morales et al. The authors explain the usage of sliders to overcome obstacles. Clamps are fixed on a subsequent step and then sliders are used to lift the robot. This mechanism is stable and it keeps the robot vertical during ascending or descending motions. Furthermore, advanced robots have also been developed which are not only able to climb the stairs but are also capable of balancing on two wheels. Ghani et al. [23] also proposed the use of two wheel clusters. In [24] Shino et al. proposed to use sliding chair along with two wheel cluster. Research was conducted to develop stair climbing robots by using rotating multi-limb structure [25]. Moreover, a mechanism based on four bar parallel links was developed [26]. Furthermore, researchers have also worked on cluster based stair climbing robots in which a single wheel is replaced by a cluster of three wheels. These wheel clusters are connected to the body of the robot at the centroid of a triangle formed by those wheels. Through a series of articles, Quaglia et al. illustrated a step climbing robot which comprised two pairs of clustered wheels [27–29]. In order to improve the mobility of the robot, a modular approach was implemented [30,31]. In order to improve stability of the climbing robot, the front pair of wheel cluster was replaced by a track-belt assembly [32–34]. As we may notice, many stair climbing robots are developed and can climb up or down the stairs; however, these systems have their own shortcomings. Robots with track-belts are efficient in climbing the stairs but are relatively slower in planes in comparison to wheel-based systems. In cluster-based and hybrid robots, the inclination angle varies drastically, limiting the robot to carry objects possessing a low center of gravity. Maintaining the inclination angle of the robot parallel to the ground is important while carrying a liquid or semi-liquid product. Hence, in this article, a novel robot is proposed, wherein two motors are attached to the front wheels of the robot and another one to the rear wheel along with an actuator, which is responsible for controlling the variation in the inclination angle of the robot. While climbing up the stairs, maintaining a proper inclination angle results in establishing a better grip between the wheels and the edge of the stairs. This reduces the risk of slippage. On the other hand, maintaining a proper inclination angle during descending reduces the probability of toppling, resulting in the improved stability of the robot. The fundamental question that we wanted to address in this study is whether the performance of the system (stair climbing robot) improves in terms of stability and dynamic equilibrium by adding a minimalistic linkage mechanism. A qualitative comparison of existing step climbing mechanisms is presented in the Table 1. Initial work towards the development of the proposed mechanism is available in the open literature [35]. In [36], the mathematical formulation and preliminary experiment results of the proposed mechanism were discussed. In the subsequent sections, details of the proposed mechanism, simulation and experimental results are explained.

**Table 1.** Qualitative comparison of existing step climbing mechanism.

Mechanisms	Advantages	Disadvantages
Tracked based [1]	Successful operation on stairs and irregular terrains	Slower in horizontal plane
Articulated leg [4]	Stable design to climb stairs	Complex control design and slower in horizontal plane
Tracked based hybrid [5]	Successfully climbs on stairs as well as fast on planes	Two separate mechanism results in heavier system
Articulated leg based hybrid [6]	Stable in climbing stairs and fast in horizontal plane	Higher power consumption
Two wheel cluster [23]	Autonomous operation on stairs	Required assistance during step climbing
Three wheel cluster [27]	Successfully climbs on stairs	Unstable during operating on uneven stairs
Proposed mechanism	Simple and minimalist design	Increased length of the system limits the system to operate in confined space

This paper is organized in the following manner: Section 2 explains the working principle; Section 3 defines the design parameters and modeling of the robot. In Section 4, the analysis of the effects of various parameters of a climbing robot is studied; in Section 5, development of a prototype and the results of experiments on the prototype are discussed. In Section 6, the importance of controlling the inclination angle of a robot while climbing a stair is explained. Section 7 concludes the article.

## 2. Working Principle

This section explains the proposed mechanism of the stair-climbing robot. Figure 1a shows a schematic of a series of actions taken by the robot while ascending the stairs, whereas Figure 1b describes the descending process of the robot of the stairs. The proposed robot has two large front wheels and one small rear wheel. The rear wheel is connected to the body of the robot by a connecting link and a revolute joint. The angle between the connecting link and the body is varied to maintain the inclination angle of the body while ascending or descending the stairs.

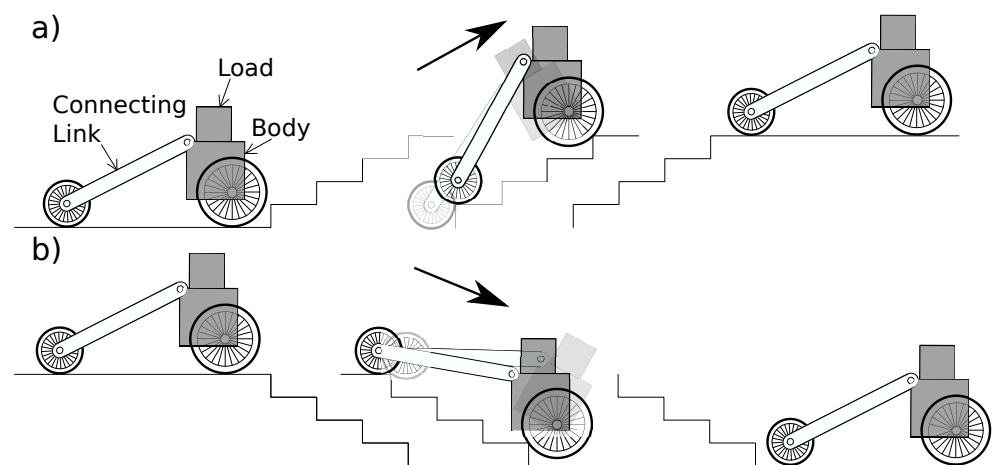


**Figure 1.** Schematic showing different positions of the robot (it may be noted that the front wheel diameter is larger than the step height); (a) ascending the stairs; (b) descending the stairs.

In Figure 1a, the left image represents the condition when both rear and front wheels are on the ground, while the middle figure refers to the situation when the front wheels

and rear wheels are on the step. The light shaded image of the robot represents the position of the robot in which the angle between the body and the connecting link is kept constant during the entire climbing operation. The right image on the figure shows the position of the robot after completion of the climbing operation. Similarly, Figure 1b illustrates changes in the posture of the robot while descending the steps.

It may be noted, if the angle between the connecting link and the body of the robot remains constant, the inclination of the body with respect to the horizontal will vary as the robot progresses on the steps. During the ascent and descent, the inclination angle of the body will tend to increase and decrease, respectively. During the descent, depending on the configuration of the robot and steps, the inclination angle may reduce to a negative value which may cause the robot to topple. This situation can be avoided by controlling the angle between the connecting link and the body of the robot.

In order to compensate for the change in the inclination of the robot, an additional servo motor is used at the joint between the body and the connecting link while climbing on the steps. This servo motor is actuated by a microcontroller whenever a change in the inclination angle of the body is detected. An IMU is used to track any change in angle during the motion of the robot. These signals are fed to a microcontroller, which in turn controls the actuator. As a result, the inclination angle of the robot is properly maintained. In the following section, the design and modeling of the robot are discussed.

### 3. Design and Modeling

A mathematical model is developed, to analyze the kinematic and dynamic behavior of the robot during its ascent and descent of a stair. This section describes the relationship between various components of the robot. Moreover, the equations for the trajectory of the wheel on steps are discussed. Finally, a method to determine the minimum length of the connecting link for the successful operation of the proposed robot is explained.

#### 3.1. Design Parameters

This section illustrates the terms used to define the proposed robot. Figure 2a shows schematic of the proposed robot. Figure 2b illustrates the linkage representation of the robot. A five-link mechanism is used to describe the proposed robot. The encircled numbers represent the link numbers. Point A and E represent the two contact points of the front and rear wheel on the stairs, respectively. Points B, C and D represent various revolute joints connecting the body to the front wheel, the body to the connecting link and the connecting link to the rear wheel, respectively. The center of gravity of the body and the load is considered to be acting at point F and G, respectively. Figure 2c shows the top view of the proposed robot.

$$\theta_3 = 270^\circ + \sin^{-1} \left( \frac{\sqrt{l_3^2 - (l_{1y} + l_2 \sin(\theta_2^0 - \theta) + (A_y - B_y))^2}}{l_3} \right) \quad (1)$$

The relation between the angle of connecting link with the horizontal and the inclination angle of the robot is given by Equation (1), where  $\theta_2^0$  is the angle of link 2 with the horizontal when  $\theta = 0^\circ$ .

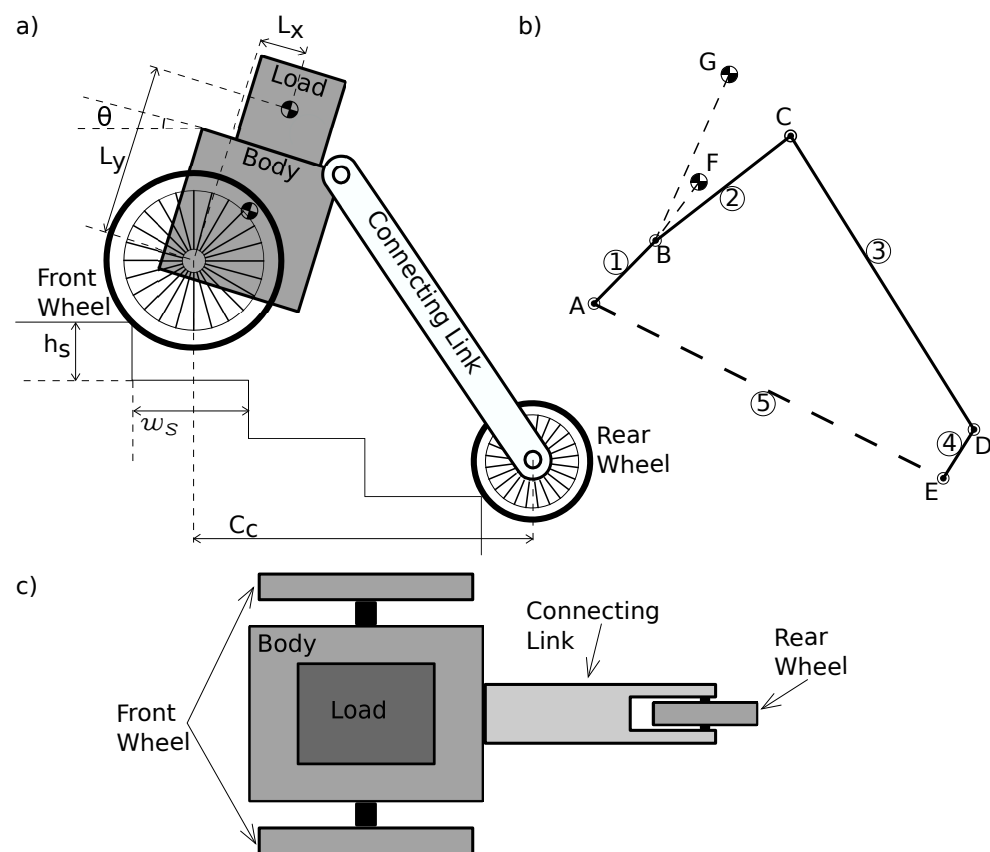


**Figure 2.** (a) A schematic view of the stair climbing robot; (b) Robot as a 5 bar linkage mechanism; (c) Top view of the robot.

### 3.2. Locus of the Center of Wheel While Ascending/Descending the Stairs

The motion of the robot depends on the trajectory of the wheel center on the steps. It is found that the pattern of the trajectory depends upon the radius of wheel as compared to height of the step. This can be categorized into two groups, which are the following: radius of wheel larger than or equal to height of the step and the other group being the radius of wheel smaller than height of the step. In the following section, equations of the corresponding paths followed by the wheels are discussed.

Figure 3 illustrates the path traced by center of the wheels. The trajectory shown in solid lines represents that of a wheel, for which its radius ( $R$ ) is equal to or greater than the height of a single step ( $h_s$ ), whereas the path in dotted lines represents the trajectory of a wheel for which its radius ( $r$ ) is less than  $h_s$ .

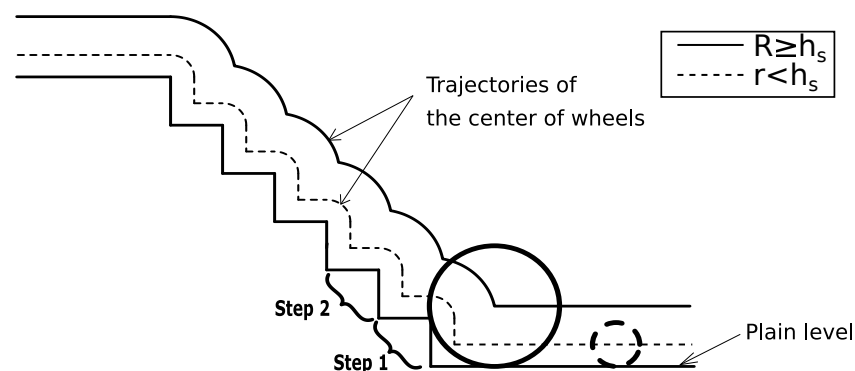


**Figure 3.** Locus of the wheel center on steps.

It can be observed from Figure 3 that the center of the wheel traces a linear horizontal path until the wheel touches the edge of the step. Thereafter, in the case of the wheel

possessing a radius larger than or equal to the height of the step, the center of wheel traces a circular path with the edge of the step as the center and radius  $R$ . Since the motors of front wheel and rear wheel are attached to the frame, any oscillation of the frame will result in respective changes in the angular velocities of the wheel. Hence, the angular velocities of the wheels are determined by using Equation (7). In the following section, equations of the path traced by the front and rear wheels are discussed.

### 3.2.1. Case 1: Radius of Wheel Is Greater than Height of Step

Figure 4 shows the schematic of the condition where the radius of the wheel is greater than the height of the obstacle.

$$\begin{aligned} OA &= R_w - h_s \\ AB &= \sqrt{OB^2 - OA^2} \\ &= \sqrt{R_w^2 - (R_w - h_s)^2} \end{aligned}$$

$R_w$  = Radius of wheel

$h_s$  = Height of step

$\omega$  = Angular velocity of the wheel

Let  $(x_o, y_o)$  be the coordinates of point  $O$  (center of wheel) and  $(x_i, y_i)$  be the coordinates of the vertex of the step, where  $i$  is the step number on which the wheel is climbing.

$$y_o = \begin{cases} R_w, & \text{if } AB > x_o - x_i \\ \sqrt{R_w^2 - (x_o - x_i)^2}, & \text{if } AB \leq x_o - x_i \end{cases} \quad (2)$$

Equation (2) illustrates that the center of the wheel moves in a straight line with zero slope until the horizontal distance between the wheel center and vertex of step is less than  $AB$ , i.e., when the wheel touches edge of the step. After that center of the wheel moves in a circular path, with  $(x_i, y_i)$  as its center and  $R_w$  as the radius of the circular path.

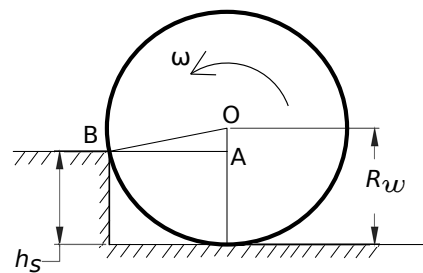


**Figure 4.** Schematic representation of step and wheel  $R_w \geq h_s$ .

Once the wheel starts to move in a circular path, the step count is incremented to the next step and the cycle continues until the last step.

### 3.2.2. Case 2: Radius of Wheel Is Lesser than or Equal to Height of Step

When the radius of wheel is smaller than the height of a single step, most parts of the equation hold true from the above case. However, in between the linear horizontal and circular path, a linear vertical path is introduced in which the  $y$ -coordinate will be incremented by  $\Delta y$ . This path continues until ' $y$ ' coordinate of the wheel center becomes smaller than the height of the current step. The equation of the path is described as follows.

$$y_o = \begin{cases} i * h_s + R_w, & \text{if } AB > x_o - x_i \\ y_o + \Delta y, & \text{if } y_o < i h_s \ (\Delta y = \omega R_w) \\ \sqrt{R_w^2 - (x_o - x_i)^2}, & \text{if } AB \leq x_o - x_i \end{cases} \quad (3)$$

### 3.3. Length of the Link in Linear Actuation

The inclination angle of the robot is regulated by rotating the connecting link with respect to the body of the robot. In this section, the procedures for calculating the minimum length of the connecting link required for successfully climbing the stairs are discussed. Figure 5 shows a position of the robot where  $\theta_1 = 90^\circ$  and  $\theta = 0^\circ$ . For a given  $\psi$ , the minimum length of the connecting link is obtained by the following procedure.

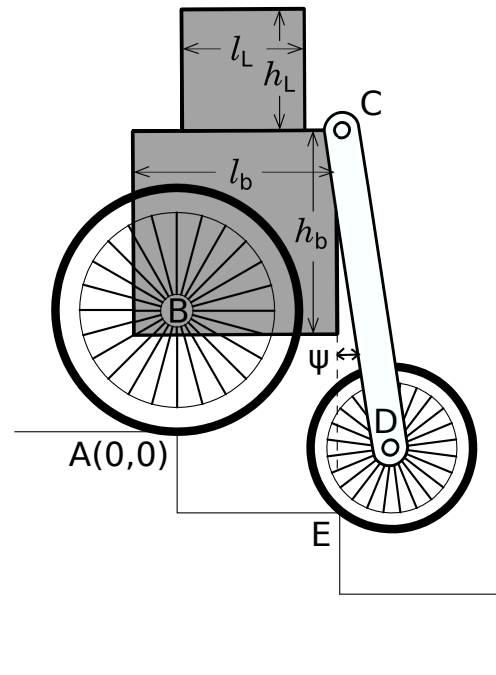


Figure 5. Schematic for actuator length calculation while ascending.

Considering the contact point of the front wheel and the stair as the origin, the coordinates of the points B and C are  $(0, l_1)$  and  $(l_2 \cos \theta_2, l_1 + l_2 \sin \theta_2)$ , respectively. The location of point D is the solution of the line passing through point C possessing a slope of  $\tan(270^\circ + \psi)$  and the Equation (2) or Equation (3) (depending on the radius of the rear wheel). The length of the connecting link is given by Equation (4).

$$l_3 = \sqrt{(D_x - C_x)^2 + (D_y - C_y)^2} \quad (4)$$

### 3.4. Kinematics of the Robot

Kinematic analysis is performed for a robot to establish a relation between the relative motion of the links. The simplified kinematic model of the proposed robot is represented by rigid links as shown in Figure 6, where the front and rear wheel are represented by link AB and DE, respectively. Assuming the no-slip condition during the motion of the wheels at the edge of a step, the point of contact between the wheel and step is considered as a resolute joint for performing kinematic analysis. When the wheels are moving over the horizontal surface, the respective links connecting the center of the wheel and the contact point is considered perpendicular to the surface. In the following section, equations describing position, velocity and acceleration of the links are shown.

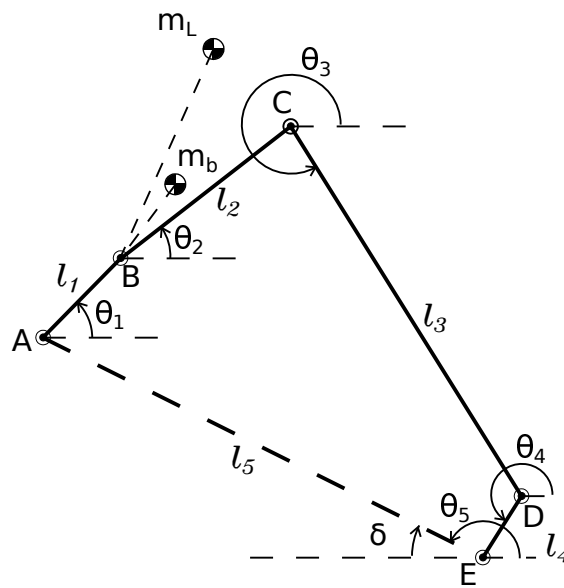


Figure 6. Kinematic model of the robot.

#### Position, Velocity and Acceleration

The position, velocity and acceleration of the links are illustrated with the help of Equations (6)–(8). The length of links AB, BC, CD and DE are system parameters. The location of point A and E are given by  $(A_x, A_y)$  and  $(E_x, E_y)$ , respectively.

$$\begin{aligned}
 l_5 &= \sqrt{(A_x - E_x)^2 + (A_y - E_y)^2} \\
 \theta_5 &= \arctan\left(\frac{A_y - E_y}{A_x - E_x}\right) \\
 \beta &= \pi - \theta_5 \\
 \theta_{12} &= \theta_2 + (\pi - \theta_1) \\
 \theta_{34} &= \theta_4 - \theta_3 + \pi
 \end{aligned} \tag{5}$$

Since  $\theta_{12}$  and  $\theta_{34}$  are the input angles,  $\theta_2$  and  $\theta_3$  are derived by equating real and imaginary parts of the position equation of the kinematic chain.

$$l_1 e^{j\theta_1} + l_2 e^{j\theta_2} + l_3 e^{j\theta_3} + l_4 e^{j\theta_4} + l_5 e^{j\theta_5} = 0 \tag{6}$$

The corresponding velocity equations may be expressed as the following.

$$l_1 j\omega_1 e^{j\theta_1} + l_2 j\omega_2 e^{j\theta_2} + l_3 j\omega_3 e^{j\theta_3} + l_4 j\omega_4 e^{j\theta_4} + l_5 j\omega_5 e^{j\theta_5} = 0 \tag{7}$$

The corresponding acceleration equation may be expressed as the following.

$$\begin{aligned}
 l_1(j\alpha_1 - \omega_1^2)e^{j\theta_1} + l_2(j\alpha_2 - \omega_2^2)e^{j\theta_2} + l_3(j\alpha_3 - \omega_3^2)e^{j\theta_3} + l_4(j\alpha_4 - \omega_4^2)e^{j\theta_4} + l_5(j\alpha_5 - \omega_5^2)e^{j\theta_5} = 0
 \end{aligned} \tag{8}$$

The unknowns  $\omega_2$ ,  $\omega_3$ ,  $\alpha_2$  and  $\alpha_3$  are determined by solving Equations (7) and (8), which may be used in dynamic analysis for deriving the forces at joints.

#### 3.5. Dynamics of the Robot

In this section, the dynamic equations of the proposed robot are developed. These equations help in analyzing the forces on different links, which are caused due to the weight of the system, payload and motion of system on the stairs. In order to develop the equations, the Newton–Euler method is used. The free body diagram of members of the robots are shown in Figure 7.

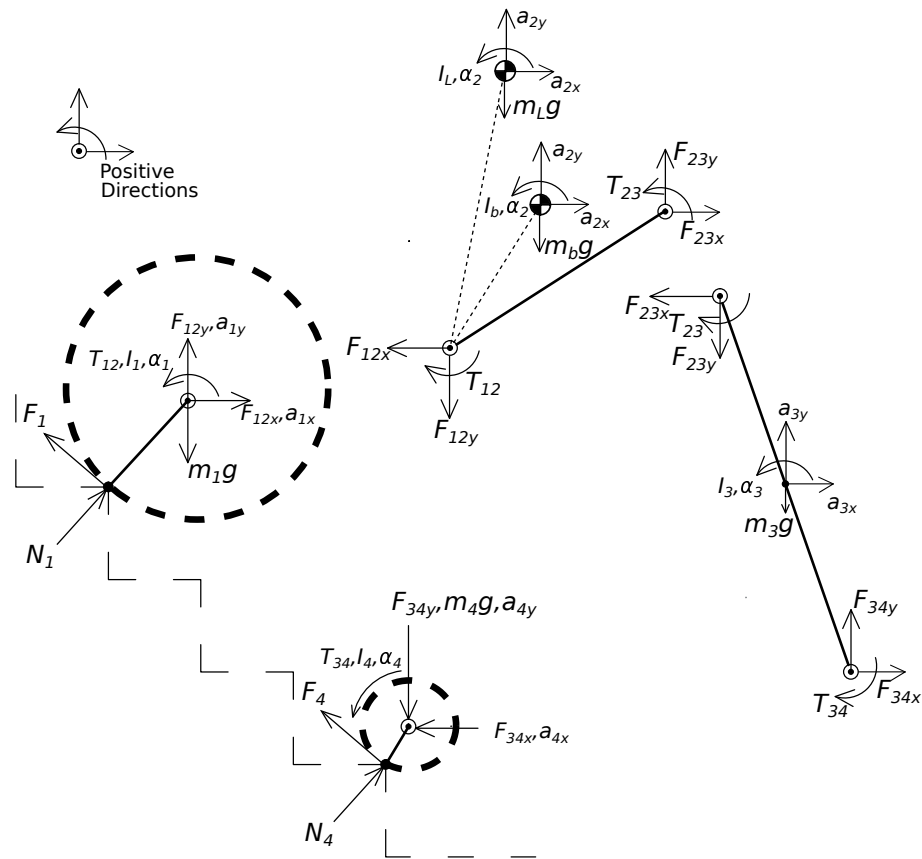


**Figure 7.** Free body diagram of the members of robot.

### 3.5.1. Equation of Motion of the Robot

For developing the dynamic model of the robot, we have considered a case where both the front and rear wheel are rolling on edges of the stairs. Different cases of complete motion of the robot can be represented by setting the angles  $\theta_1$  and  $\theta_4$ . For example, when the front wheel is moving horizontally,  $\theta_1$  is set to  $90^\circ$ . Similarly, dynamic model of the robot is altered depending on the motion of wheels. The derived equation of motion in matrix form is presented in Appendix A.

### 3.5.2. Equation of Motion of Wheel

This section explains the derivation of the equation of the motion of the wheel. Figure 8 shows the free body diagram of a wheel when torque ‘T’ is applied at the center of the wheel. The angle made by the line joining the instantaneous center of the rolling wheel and the center of the front wheel with the horizontal is  $\delta$ . If the wheel moves forward without any slip between the wheel and track surface, then the relative velocity of the wheel at contact point ‘C’ (between wheel and track) will be Zero. Hence, the forward motion is only caused by the static frictional force and the frictional force ( $f_f$ ) will be in the direction of forward motion of the wheel. The equation of motion of the wheels are given by Equations (9)–(12).

$$N_w \cos \delta - f_f \sin \delta - f_x = m_w a_x \quad (9)$$

$$N_w \sin \delta + f_f \cos \delta - m_w g - N = m_w a_y \quad (10)$$

$$T = f_f * OA + I\alpha \quad (11)$$

$$T_{allowable} = \mu_s * N \quad (12)$$

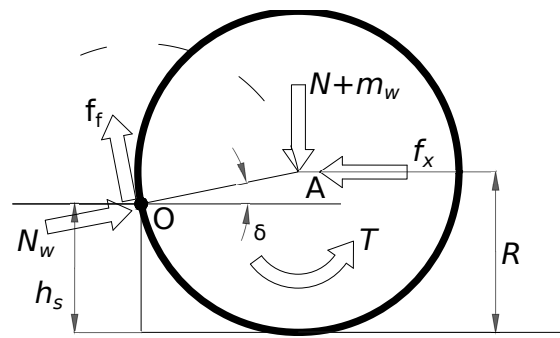


Figure 8. Free body diagram of wheel.

#### 4. Design Analysis

In Section 3, the equations for describing the mathematical model of the proposed robot are discussed. The contribution of various parameters of the robot must be studied for successful operation of the robot on the stairs. In this section, the contribution of the parameters of a robot on the stairs is illustrated. The dimensions of the robot and the stairs are shown in Table 2. For the analysis, one of the parameters is varied while keeping the other parameters unchanged.

Table 2. Dimension of the robot for analysis.

Parameters	Values	Parameters	Values
R	300 mm	$m_1$	10 kg
r	200 mm	$m_4$	5 + 45 (Pay load) kg
$l_b \times h_b$	400 × 300 mm	$m_b$	10 kg
$l_L \times h_L$	150 × 200 mm	$m_L$	150 kg
$L_3$	800 mm	$m_3$	5 kg
$L_x$	325 mm	$\mu_s$	0.7
$h_s$	160 mm	$w_s$	240 mm

When the robot climb stairs, the inclination angle of the robot changes significantly. With little consideration, it may be observed that the change in inclination angle depends on various parameters of the robot and the stair. One of the parameters that influence the variation in the inclination angle is the height of the step of a stair. Figure 9 illustrates the change in inclination angle of the robot at three initial steps of the stairs when the height of the step is varied from 70 mm to 160 mm. The three plots, step 1, step 2 and step 3, represent the variation of inclination angle when the front wheel is at the first, second and third steps of the stair and the height of the step is varied from 70 mm to 160 mm, respectively. It may be noticed that, in step 1, although the contact point of the step edge with the front will raise with an increase in step height, the robot inclination angle remains unaffected. It is observed that with the increase in step number, the slope of the plot, which represents the change in inclination angle of the robot, also increases.

In Figure 9, as the height of a step increases, the torque required by the front wheels to overcome the step will also increase. Although higher torque required by the front wheels may be achieved by selecting higher torque motors, the maximum allowable torque on the front wheel is directly proportional to the product of the coefficient of static friction and the normal reaction of the wheel at the contact point between the edge and the wheel (Equation (12)). If the torque on the front wheels exceeds the maximum permissible limit, the front wheel will slip on the edge of the step, resulting in failure in climbing the stairs. The variations in the required torque and maximum allowable torque with respect to the change in step height at three initial steps are shown in Figure 10. In Figure 10a, the effect of step height on the torques of the front wheels is shown when the simulations are performed while controlling the inclination angle of the robot in climbing up the stairs, whereas Figure 10b illustrates the simulations without controlling the inclination angle. It

may be observed that in both the controlled and uncontrolled simulations, the required torque increases along with the height of the steps, whereas the maximum allowable torque decreases. However, in the controlled case, the torque required to overcome the step is lower than the maximum allowable torque, whereas the required torque is higher than the maximum allowable torque in the uncontrolled case. This will result in slippage of the front wheel during uncontrolled operations.

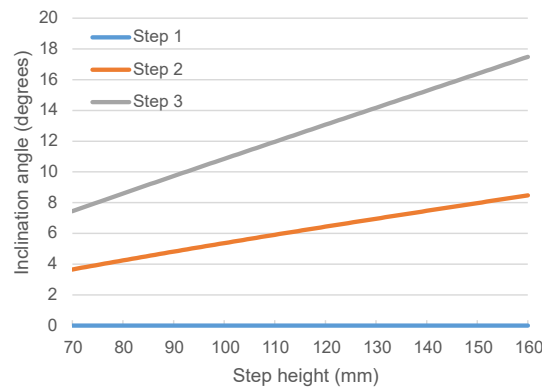


**Figure 9.** Variation of inclination angle of the robot with a change in height of a step at three initial steps of the stair during the operation of climbing up the stairs. The three plots, step 1, step 2 and step 3, represent the variation of inclination angle when the front wheel is at the first, second and third step of the stair, respectively.

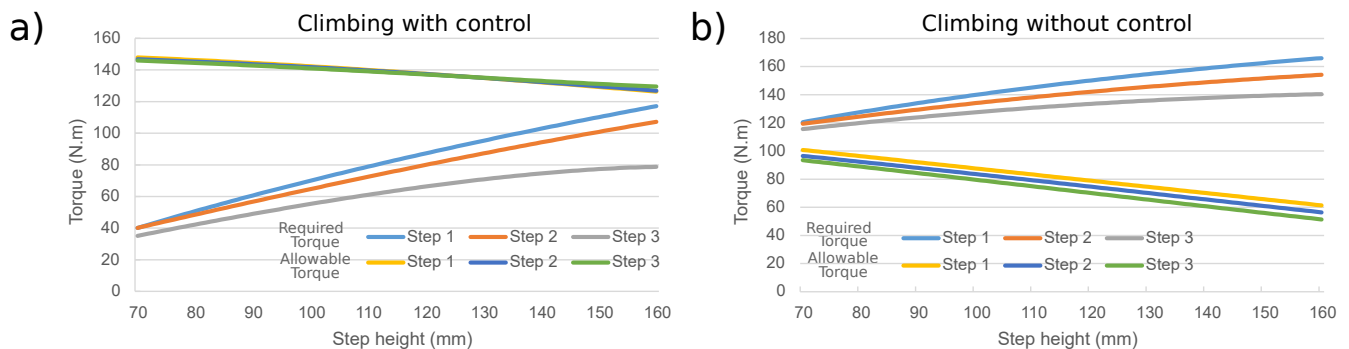


**Figure 10.** Change in allowable and required torque on the front wheels to overcome a step with respect to the change in height of the step while (a) climbing with control and (b) climbing without control.

In Figure 10, the uncontrolled simulations are performed with passive rear wheels, whereas controlled simulations are performed with active rear wheels. It may be noticed that during uncontrolled simulations, the maximum allowable torque on the front wheels is less than the required torque, resulting in the slippage of front wheels. In Figure 11, the behavior of the climbing robot during uncontrolled and controlled simulations with active rear wheels is studied. The statistical analyses of variation in the difference of required and allowable torque in the front wheels during controlled and uncontrolled conditions with respect to change in height of step are shown in Table 3. It may be observed that the mean values of required torque on step 1, 2 and 3 are 64.66 Nm, 63.68 Nm and 69.21 Nm, respectively. This implies that, during uncontrolled conditions, more torque is required to overcome a step as compared to the controlled condition. The standard deviation value for each step suggests that the required torque in the uncontrolled condition is always higher than the controlled condition, when simulations are performed with respect to the varying height of the stair. Similarly, negative mean values of allowable torque imply that the allowable torque in an uncontrolled condition is smaller as compared to the controlled condition. Moreover, standard deviation values show that the allowable torque always remain higher in the controlled condition. This reduces the probability of slipping during

controlled conditions as compared to the uncontrolled condition. Figure 11a illustrates the variation in allowable and required torque at three initial steps on the front wheels with a change in step height. By comparing the results of an uncontrolled simulation with the active rear wheel (as shown in Figure 11a) and the controlled simulations with the active rear wheel (as shown in Figure 10a), it may be observed that as the step number increases, the required torque to overcome the step in uncontrolled simulations become lesser than compared to the controlled conditions. In Table 4, the mean values and standard deviation values of variation in difference of required and allowable torque in the front wheels during controlled and uncontrolled conditions with active rear wheel and with respect to change in height of step are shown. It may be observed that the mean values of difference in the required torque between uncontrolled and controlled condition are negative and the difference becomes smaller with the increase in step number. By Analyzing the mean values with standard deviation values implies that although the required torque in uncontrolled condition is smaller than the controlled condition at lower steps, as the step number increases, the required torque in the front wheels becomes smaller in the controlled condition as compared to the uncontrolled condition. This phenomenon is observed as the inclination angle of the robot increases with the step number. By analyzing the mean and standard deviation values of allowable torque, it may be observed that as the step number increases, the allowable torque in the controlled condition increases and deviates less than compared to lower step number. In order to understand this behavior, the variations in maximum allowable torque on the rear wheel in both controlled and uncontrolled conditions are plotted and shown in Figure 11b. It may be observed that except for the condition where the front wheels are on the third step and the step height is over 150 mm (approximately), the maximum allowable torque on the rear wheel in the uncontrolled condition is greater than the controlled condition. The torque on the rear wheel pushes the robot, which in turn accounts for the decrease in torque requirement on the front wheels. Hence, the higher the rear wheel torque, the lower the torque will be that is required by the front wheels for climbing over an obstacle. Table 5 shows the mean and standard deviation values of difference in allowable torque during the uncontrolled and controlled condition in the rear wheel with an increase in step number and change in height of the step. The decreasing value of mean and increasing value of standard deviation with higher step number implies that with the increase in the step number and the height of the step, the allowable torque in the controlled condition becomes higher than that of uncontrolled condition.

**Table 3.** Statistical analysis of variation in difference of required and allowable torque on front wheels during controlled and uncontrolled conditions with respect to the change in the height of a step.

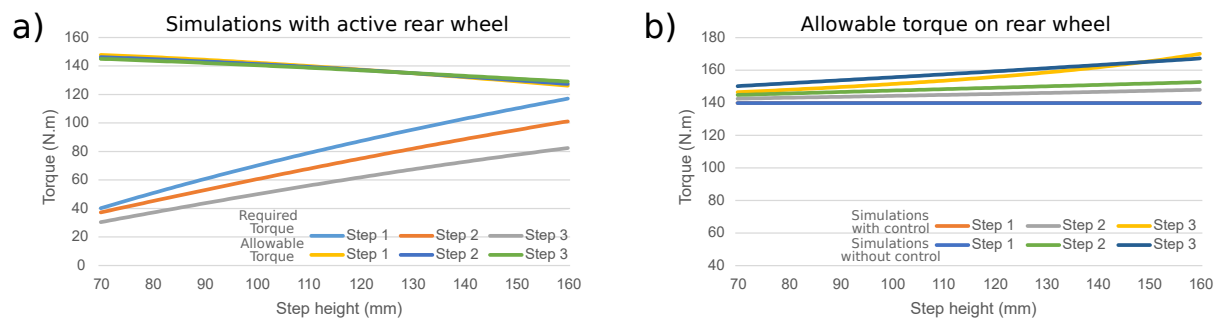
	Required Torque (Nm)			Allowable Torque (Nm)		
	Step 1	Step 2	Step 3	Step 1	Step 2	Step 3
Mean	64.66	63.68	69.21	−57.18	−61.22	−65.47
Std. Dev.	9.17	9.46	5.92	5.15	5.91	7.38

**Table 4.** Statistical analysis of variation in difference of required and allowable torque on front wheels during controlled and uncontrolled conditions with an active rear wheel and with respect to change in height of step.

	Required Torque (Nm)		Allowable Torque (Nm)	
	Step 2	Step 3	Step 2	Step 3
Mean	−4.69	−3.44	−0.11	−0.30
Std. Dev.	0.93	2.45	0.33	0.30

**Table 5.** Statistical analysis of variation in the difference of allowable torque on the rear wheel during controlled and uncontrolled conditions and with respect to change in the height of the step.

	Allowable Torque (Nm)	
	Step 2	Step 3
Mean	3.61	2.66
Std. Dev.	0.70	1.90

**Figure 11.** Simulation with an active rear wheel; (a) Change in allowable and required torque on front wheels to overcome a step with respect to the change in height of the step (without controlling the inclination angle); (b) variations in allowable torque on rear wheels when the front wheels overcome steps with the varying height of the step.

The simulation conditions for the results plotted in the Figures 10 and 11 corresponds to a situation where the front wheel is considered on a step whereas the rear wheel is on a plane surface. Moreover, the height of the carried load is kept constant in the simulations. For a climbing robot, one of the most challenging conditions is when both the front and rear wheels overcome the steps simultaneously. In Figure 12, the effect of the height of the center of gravity of load is illustrated when both the front and rear wheels are at the edge of the steps. The height of the center of gravity of the load is varied from 50 mm to 1300 mm. The simulations for the cases wherein the inclination angle is actively controlled are performed for step 2 and step 3, only as the simulations at step 4, to maintain the inclination angle of the robot; the rear wheel has already climbed over the step 1. Figure 12a,b illustrates the variation in torque requirement in the front and rear wheels, respectively. It may be observed in Figure 12a that the required torque to overcome the step decreases in the case of controlled simulations as the front wheels are placed on higher steps. This phenomenon occurs because the connecting link is rotated to maintain the inclination angle, which in turn reduces the horizontal center distance of the front and rear wheels. As the center distance decreases, the center of the load proceeds closer to the rear wheel and a higher percentage of vertical load is shared by the rear wheels as compared to the front wheels. Moreover, the required torque on front wheels remains constant even with the increase in the height of the center of gravity (of the load). However, in the case of uncontrolled conditions, the variations in the required torque (required by the front wheels to overcome a step with respect to the changing heights of the center of gravity of the load) possess a negative slope. Moreover, the slope decreases with every higher step number. Eventually, the torque reduces to a negative value at the fourth step, while the height of the center of gravity (of the load) is close to 1300 mm. The negative value of the torque signifies that the normal reaction on the front wheels has decreased to a negative value and the robot will topple due to the moment produced by the load. As the normal reaction on the front wheel during uncontrolled stimulation decreases, the normal reaction on the rear wheel will increase, which is shown in Figure 12b. The statistical analyses of variation in the difference of required and allowable torque in the front wheels during controlled and uncontrolled conditions with respect to the height of the center of gravity of load are shown in Table 6. The negative mean value for the difference in required torque implies that the required torque in the uncontrolled condition is less than controlled condition and

the difference increases with an increase in step number as well as the height of the center of gravity of the load. The reason for this phenomenon is, as the step number increases in the uncontrolled condition, the inclination angle also increases, which results in a higher percentage of load shared by the rear wheel than compared to the front wheels. Hence, the difference between the required torque on the rear wheel increases with an increase in step number. This shows that the required torque in the rear wheels during the uncontrolled condition is higher than the controlled condition.

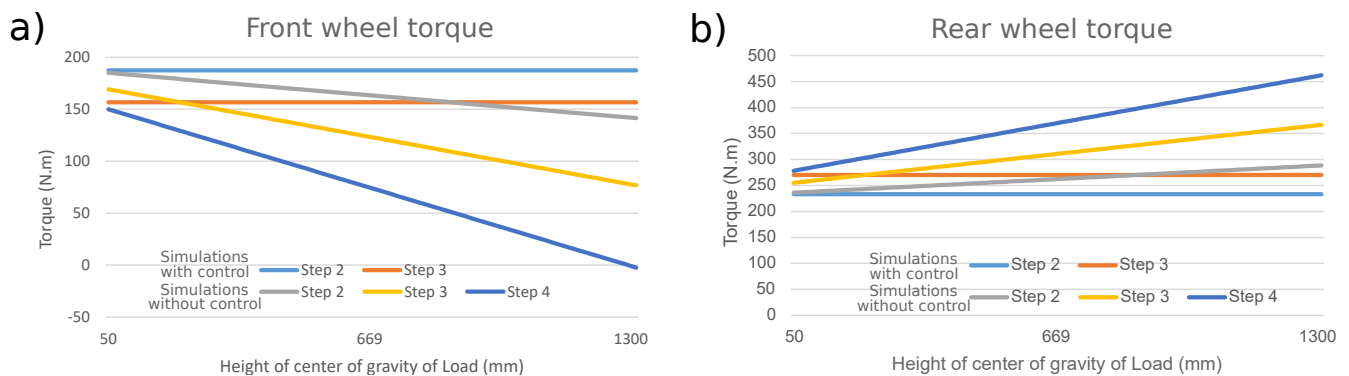


**Figure 12.** Simulation with an active rear wheel when both the front and the rear wheel are on the edge of a step (a) change in required torque on the front wheels with respect to the height of the center of gravity of the load; (b) change in required torque on the rear wheel with respect to the height of the center of gravity of the load.

**Table 6.** Statistical analysis of variation in difference of required torque on the front and rear wheels during controlled and uncontrolled conditions with respect to center of gravity of load.

	Required Torque (Nm)			
	Front Wheel		Rear Wheel	
	Step 2	Step 3	Step 2	Step 3
Mean	−24.26	−33.73	29.27	40.69
Std. Dev.	12.70	26.99	15.32	32.55

While the robot is climbing up the stairs, gravity acts against its motion which makes the ascending motion on the stairs difficult in comparison to the descending. However, while the robot is climbing down a stair, its inclination angle is an important parameter since, beyond a certain inclination angle, the robot may topple. In Figure 13, the variation of the inclination angle (of the robot) with respect to the change in height of the steps at three initial steps (from the top) is plotted. The first step on the stair (after the top platform) is referred as textbf step 1, whereas textbf step 2 and textbf step 3 are the subsequent steps. It may be observed that as the height of the step increases, the inclination of the robot decreases. The slope of the plot showing variation in the inclination decreases with an increase in step number.

One of the important parameters for the successful descent of the robot is the height of the center of gravity of the load. In order to analyze the effect of height of the center of gravity of the load, the variation in the normal reaction on the rear wheel of the robot is illustrated in Figure 14. It may be observed that, during the controlled simulation, the inclination angle of the robot remains unchanged and the variations in normal reaction have a constant slope. However, in an uncontrolled simulation, the inclination angle of the robot varies drastically with an increase in the center of gravity (of the load) due to the normal reaction on the rear wheel decreasing as well. This phenomenon is observed as the moment generated by the load increases with the decrease in inclination angle. It may be observed that during the uncontrolled simulation at step 4, if the height of the center of gravity (of the load) is more than 771 mm (approximately), the normal reaction on the rear wheels is reduced to a negative value. This will result in the toppling of the robot.

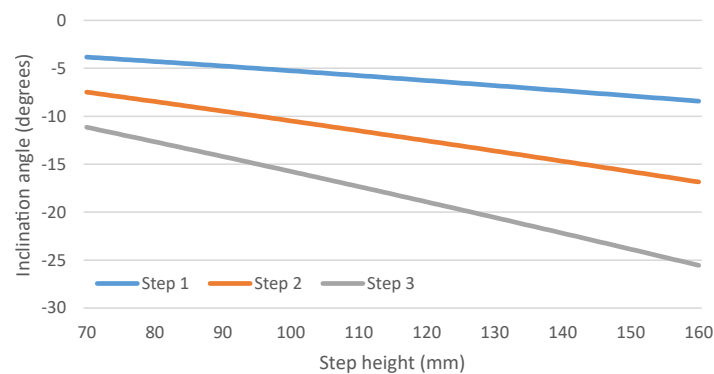


**Figure 13.** Variation of inclination angle of the robot with change in height of step during the act of climbing down the stairs.

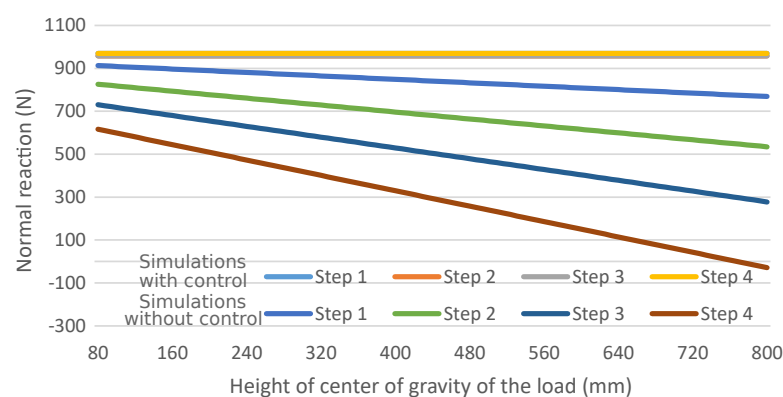


**Figure 14.** Variation of normal reaction on rear wheel with respect to change in height of the center of gravity of the load.

Table 7 shows the mean and standard deviation values of the difference in normal reaction in the rear wheel with an increase in step number and change in the height of the center of gravity. The increase in negative mean value imply that the normal reaction on the rear wheel during the uncontrolled condition becomes smaller than compared to the controlled condition as the step number increases. The standard deviation values imply that, in all the cases with increased height of the center of gravity, the normal reaction on the rear wheel is smaller in the uncontrolled condition than compared to the controlled condition.

**Table 7.** Statistical analysis of variation in difference of normal reaction at the rear wheel during the controlled and uncontrolled conditions with respect to center of gravity of load.

	Normal Reaction (N)			
	Step 1	Step 2	Step 3	Step 4
Mean	−128.93	−277.34	−453.69	−676.34
Std. Dev.	42.09	84.94	131.98	188.12

## 5. Proof of Concept Model

By using design analysis, it was found that robots with fixed center distance between the front and rear wheels fail to carry a load with a high center of gravity while climbing a stair. In order to realize the phenomenon, a scale-down prototype is developed and experiments are performed on steps. In Figure 15, an image of the model is shown. Table 8 describes different parts of the model. The prototype consists of two front wheels and a rear wheel. The rear wheel is connected to the body by a link termed as the connecting link.

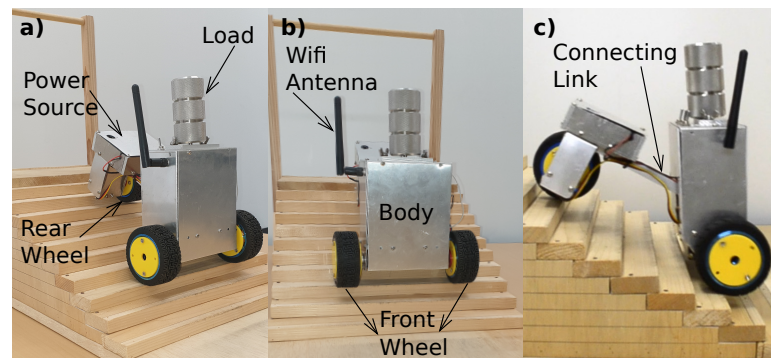


**Figure 15.** Model of the proposed robot; (a) Isometric view; (b) Front view; (c) Side view.

**Table 8.** Parts of the robot Model.

Sl. No.	Description		
1	MPU 6050 (IMU sensor) (Gyroscope range: $\pm 2000$ deg/s) (Accelerometer range: $\pm 16$ g)	7	Front Wheel ( $\phi$ 67 mm)
2	6V Power Supply	8	Load ( $\phi$ 37 $\times$ 72.75 mm; 600 gm)
3	Arduino Uno ( $\mu$ C)	9	Body (126 $\times$ 101 $\times$ 62 mm)
4	Wireless Module (nRF24L01)	10	Weight of robot (1.34 kg (without load))
5	Rear Wheel ( $\phi$ 67 mm)	11	Rise of step (15 mm)
6	Servo Motor (RDS3115MG) (Max. torque: 17.0 kgf-cm) (Max. operating angle: 180°)	12	Run of step (33 mm)
		13	Number of steps (11 mm)
		14	Connecting link (152 mm)

The electronic components used to develop the prototype are shown in Figure 16a. In the prototype, an Arduino Uno microcontroller is used as the brain of the robot. All the wheels are driven by continuous servo motors. In order to control the inclination angle, another servo motor is used which drives the connecting link of the robot. The prototype is powered by a 6V battery source. Three toggle switches are used in the robot. Switch 1 is used to connect the power source to the four motors of the robot. The power supply to the microcontroller is connected through switch 2. Switch 3 is responsible for toggling between the operating conditions of the prototype, i.e., operating with or without control.

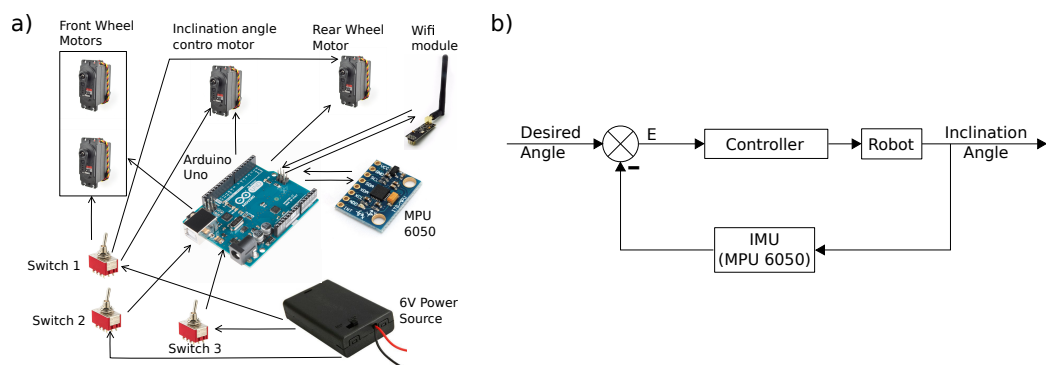


**Figure 16.** (a) Electronics components diagram; (b) block diagram of the controller.

MPU 6050 is used to sense the inclination angle of the model. The sensor consists of three Gyroscopes and three accelerometers for sensing three degrees of rotation and three dimensional spatial motions, respectively. The inclination angle of the robot is communicated to the monitor by using a wireless module. Experiments are performed for ascendance and descendance of the robot on the stairs. Figures 17–20 show the snapshots of the videos of the experiment. In order to remotely monitor the change in inclination angle of the prototype, a wifi module is used.

Figure 16b shows the flow chart of the control system that is used to maintain the inclination angle of the proposed robot. The inclination angle sensed by the inertial measurement unit (IMU) is processed by the microcontroller. Depending upon the deviation of the current inclination angle of the robot from the desired value, the microcontroller sends the actuation signals to the actuator for rotating the connecting link. By rotating the connecting link, the inclination angle of the robot is maintained at a desired value.

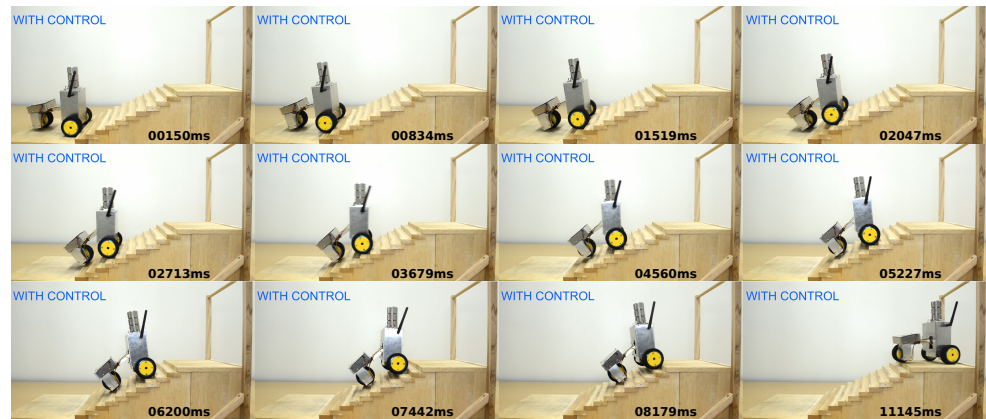


**Figure 17.** Prototype ascending with control (time stamps in milliseconds are roughly estimated from the videos).

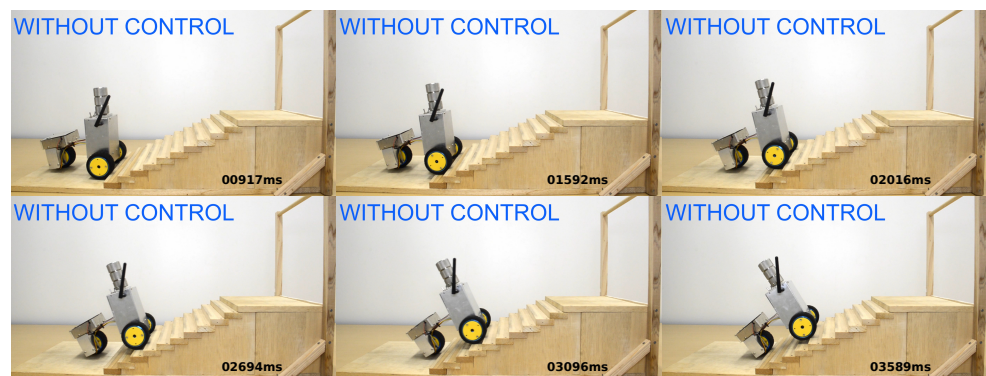


**Figure 18.** Prototype ascending without control (time stamps in milliseconds are roughly estimated from the videos).

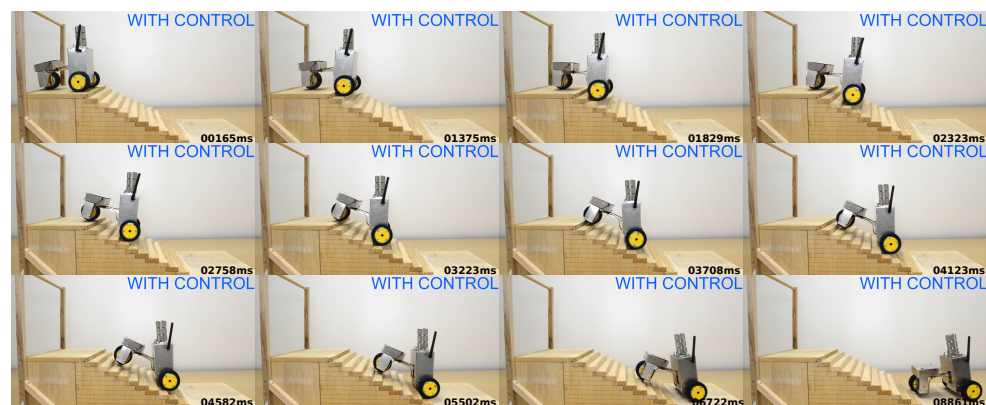


**Figure 19.** Prototype descending with control (time stamps in milliseconds are roughly estimated from the videos).

Figures 17 and 18 show the images while the model is ascending the steps. Figure 17 illustrates the case in which the inclination angle of the robot is controlled, whereas Figure 18 shows the

uncontrolled case. During the experiments, it is observed that when the inclination angle of the robot is not controlled, the robot slips on the fifth step. On the other hand, when the inclination angle is controlled, the robot successfully climb up the stairs.

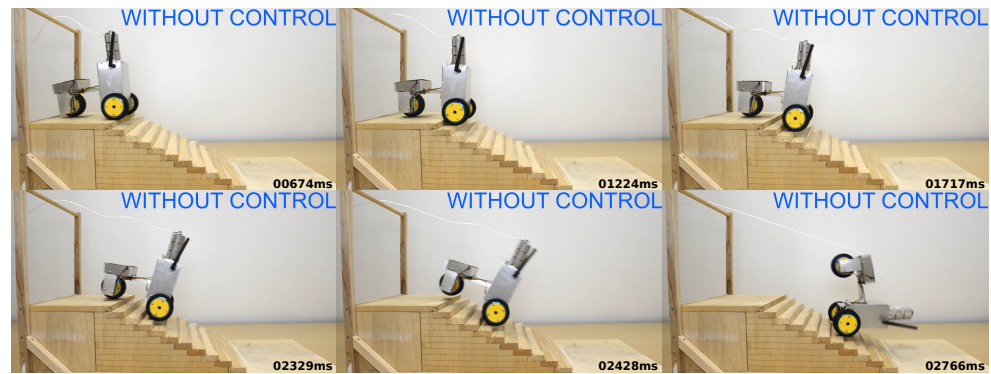


**Figure 20.** Prototype descending without control (time stamps in milliseconds are roughly estimated from the videos).

Similarly, Figures 19 and 20 show frames of the experiments, wherein the robot is descending the steps. Figure 19 represents the descendance when the inclination angle of the robot is controlled, whereas the experiment is performed without controlling the inclination angle in Figure 20. It is observed that the robot topples on the fourth step (from top) when the inclination angle is not controlled, whereas in the case of the controlled inclination angle, the robot successfully descends the stairs.

Figure 21a shows the comparison of inclination angles (of the robot) during its ascendance in controlled and uncontrolled conditions, respectively. The slope of the stair is  $24.44^\circ$ . It is observed that in the controlled condition, the maximum and minimum inclination angles are limited to  $3^\circ$  and  $-5^\circ$ , respectively. The inclination angle of the robot drops to  $-30^\circ$  during an uncontrolled setting. By using simulation, it was observed that at an inclination angle of  $-23.93^\circ$ , the front wheels and the rear wheel touch the edge of the steps. At such inclination angles, the torque, due to the high center of gravity of the load, increases to an extent that the normal reaction at the front wheels reduces to 5.29 N, whereas the normal reaction at the rear wheel increases to 22.25 N. Since the normal reaction at front wheels is low, the probability of slipping increases. During the experiments, it is observed that the slipping of wheels occurs at an angle of  $-27^\circ$ . Similarly, Figure 21b illustrates the comparison of inclination angles (of the robot) during its descendance in controlled and uncontrolled conditions, respectively. It is observed that in the controlled condition the maximum and minimum inclination angle is limited to  $6^\circ$  and  $-6^\circ$ , respectively. The inclination angle of the robot raises to  $27^\circ$  during an uncontrolled setting. Once the inclination angle reaches  $27^\circ$ , the robot topples down. By using simulation, it was found that the robot topples at an inclination angle of  $24.24^\circ$ . The difference may have happened as the inertia effect is ignored in the simulations.

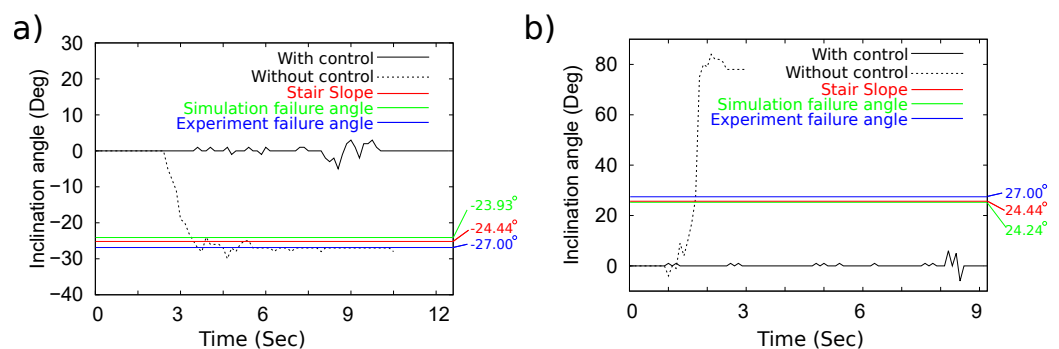


**Figure 21.** Comparison of the inclination angles of the prototype between with and without control experiments during (a) ascending on the stairs; (b) descending on the stairs.

Table 9 shows the mean and standard deviation values of difference in inclination angle of the prototype during ascending and descending experiments on the prototype with controlled and uncontrolled conditions. The negative mean value and standard deviation value during ascending show that, while climbing up without control, the inclination angle of the robot becomes negative and it decreases as the robot proceeds on the step. Similarly, the positive mean value and standard deviation value during descending show that, while climbing down without control, the inclination angle of the robot increases as the robot proceeds on the step.

**Table 9.** Statistical analysis of variation in difference of inclination angle during ascending and descending experiments on the prototype with controlled and uncontrolled conditions.

	Inclination Angle (Deg)	
	Ascending	Descending
Mean	−21.37	35.13
Std. Dev.	10.95	37.89

## 6. Discussion

In this section, the reasons for the failure of the robot during its ascendance and descendence on the stairs when the inclination angle of the robot is not controlled are discussed. Figure 22 illustrates two situations of the robot while it is climbing up on the stairs. Figure 22a shows the controlled situation while Figure 22b shows the uncontrolled situation. In the schematic, point  $G_L$  indicates the center of gravity of the load.  $\beta$  represents the angle made by a line joining the center of gravity of load and the center of front wheel ( $O$ ) with the horizontal. The subscripts of angle  $\beta$ , 'c' and 'wc' indicate the controlled and without control conditions.  $\tau$  is the torque of the motor at the front wheel. 'f' and 'N' are the frictional forces and normal reactions of the front wheel on the edge of the step, respectively.

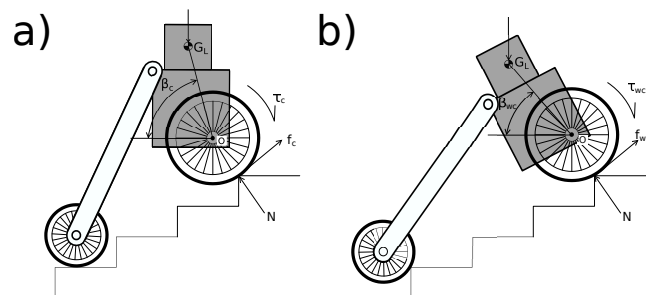


**Figure 22.** Robot schematic while ascending; (a) with control; (b) without control.

It may be observed that the following is the case.

$$\beta_c > \beta_{wc}$$

Hence, the counterclockwise moment in the uncontrolled condition (due to the center of gravity of the load) about the point  $O$  is more than that of the controlled condition. Therefore, the following is the case.

$$\begin{aligned} \tau_c &< \tau_{wc} \\ \therefore f_c &< f_{wc} \end{aligned}$$

Since the frictional force on the front wheel during the uncontrolled condition is greater than that of the controlled condition, the probability of slippage during the uncontrolled condition is greater than that of the controlled condition. Similar behavior has also been observed during the experiments.

In Figure 23, the schematic of the two situations of robot is shown while the robot is descending the stairs. Figure 23a illustrates the controlled situation while Figure 23b shows the uncontrolled situation. 'M' is the moment due to the center of gravity of load with respect to the front wheel center (O). It may be observed from Figure 23 that the moment due to the center of gravity of the load (about O) is in the counterclockwise direction during the controlled condition, whereas the moment is in the clockwise direction during the uncontrolled condition. This will result in the toppling of the robot in the uncontrolled condition, which is also observed during the experiments.

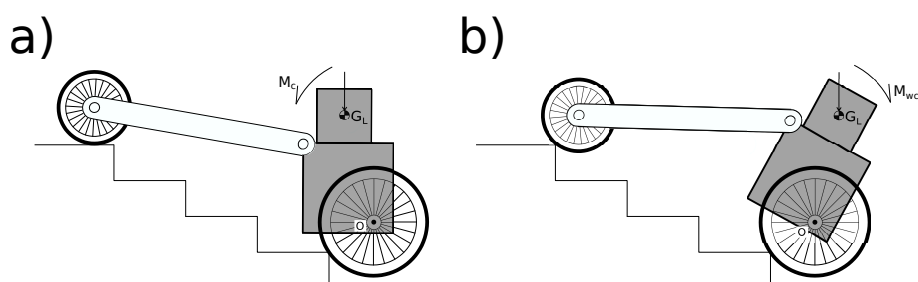


**Figure 23.** Robot schematic while descending; (a) with control; (b) without control.

## 7. Conclusions

In this article, a new mechanism for a step climbing robot is discussed and consists of two front wheels, a rear wheel and an actuator (to control the center distance between the front and rear wheels). In order to compensate for the drastic variation in the inclination angle, which can result in instability, the angle between the connecting link and the body is varied. A dynamic model (of the proposed system) is developed and various simulations are performed. During the analysis of the model, it is found that the difference between allowable and required torque on the front wheels increases by 108.5% in the controlled condition than compared to the uncontrolled condition. This reduces the probability of slipping and improved the stability of the proposed system. It is observed that the robot carrying a load with a low center of gravity and for which its front and rear wheels are connected with a rigid frame is capable of climbing up or down the stairs. On the other hand, the robot fails to climb up and down when it is carrying a load possessing a higher center of gravity. During ascending simulations with control, the required torque on rear wheel is reduced by 26.3% than compared to uncontrolled simulations. Furthermore, the normal reaction of the rear wheel during descending simulation has increased by 170.9% by controlling the inclination angle, which reduced the probability of toppling of the proposed robot. Experiments on a scaled-down prototype also reveals that the robot is unable to climb up the stairs during uncontrolled conditions whereas in controlled conditions, it can successfully climb up the stairs. By controlling the inclination angle of the prototype, the variation of inclination angle during ascending is reduced by 77.8%, whereas the variation is reduced by 92.8% during descending. Similarly, during descending experiments, it was found that the robot topples when operated without control and the robot successfully climbs down the stairs when the inclination angle was controlled.

As observed from the configuration of the system, the length of the proposed system will increase significantly due to the connecting link, which in turn will restrict such robots to operate in a confined space. In order to overcome such limitations, the connecting link should be replaced by a linear actuator. Moreover, a robust control method may be designed to enhance the performance of the robot during an external disturbance. Since cost is also a very important parameter, optimization should be performed without compromising the stability and strength of the robot. Furthermore, these models should be tested against external disturbances. Finally, full-size prototypes should be developed and experiments should be carried out to ensure the safe and stable operations of the robot.

**Author Contributions:** Conceptualization, N.J.B. and H.O.; methodology, N.J.B.; formal analysis, N.J.B. and B.B.; investigation, K.T.; resources, K.T.; writing—original draft preparation, N.J.B.;

writing—review and editing, B.B.; visualization, K.T.; supervision, H.O.; project administration, H.O. All authors have read and agreed to the published version of the manuscript.

**Funding:** This research received no external funding.

**Institutional Review Board Statement:** Not applicable.

**Informed Consent Statement:** Not applicable.

**Data Availability Statement:** Not applicable.

**Conflicts of Interest:** The authors declare no conflict of interest.

## Nomenclature

$R$	Radius of the front wheel
$r$	Radius of the rear wheel
$C_c$	Distance between centers of front and rear wheel
$\theta$	Angle of robot with horizontal (Inclination angle)
$\theta_i$	Angle of $i$ -th link with respect to horizontal
$\alpha_i$	Angular acceleration $i$ -th link
$h_s$	Height of step
$w_s$	Width of step
$A_x$	X-coordinate of point A (A is a variable)
$A_y$	Y-coordinate of point A
$\psi$	Minimum angle between link 3 with vertical
$l_{ix}, l_{iy}$	Length of $i$ -th link with respect to horizontal and vertical
$L_x, L_y$	Horizontal and vertical offset of C.G. of load from the joint between front wheel and body
$m_b, m_L$	Mass of body and load
$m_i$	Mass of $i$ -th link
$\mu_s$	Coefficient of static friction
$I_i$	Moment of inertial about C.G. of $i$ -th link
$l_i$	Length of $i$ -th link
$l_b, w_b, h_b$	Length, width and Height of the body
$l_L, w_L, h_L$	Length, width and Height of the Load

### Appendix A. Matrices of Dynamic Model of the Proposed Robot

$$A = \begin{bmatrix} \{-S\theta_1 & C\theta_1 & 1 & 0 & 0 & 0 & 0 \\ 0 & 0 & 0 & 0 & 0\} \\ \{C\theta_1 & S\theta_1 & 0 & 1 & 0 & 0 & 0 \\ 0 & 0 & 0 & 0 & 0\} \\ \{-l_1 & 0 & 0 & 0 & 0 & 0 & 0 \\ 0 & 0 & 0 & 1 & 0\} \\ \{0 & 0 & -1 & 0 & 1 & 0 & 0 \\ 0 & 0 & 0 & 0 & 0\} \\ \{0 & 0 & 0 & -1 & 0 & 1 & 0 \\ 0 & 0 & 0 & 0 & 0\} \\ \{0 & 0 & 0 & 0 & -l_2 S\theta_2 & l_2 C\theta_2 & 0 \\ 0 & 0 & 0 & -1 & 1\} \\ \{0 & 0 & 0 & 0 & -1 & 0 & 1 \\ 0 & 0 & 0 & 0 & 0\} \\ \{0 & 0 & 0 & 0 & 0 & -1 & 0 \\ 1 & 0 & 0 & 0 & 0\} \\ \{0 & 0 & 0 & 0 & 0 & 0 & l_3 S(360 - \theta_3) \\ l_3 C(360 - \theta_3) & 0 & 0 & 0 & -1\} \\ \{0 & 0 & 0 & 0 & 0 & 0 & -1 \\ 0 & -S(\theta_4 - 180) & C(\theta_4 - 180) & 0 & 0\} \\ \{0 & 0 & 0 & 0 & 0 & 0 & 0 \\ -1 & C(\theta_4 - 180) & S(\theta_4 - 180) & 0 & 0\} \\ \{0 & 0 & 0 & 0 & 0 & 0 & 0 \\ 0 & -l_4 & 0 & 0 & 0\} \end{bmatrix}$$

$S\theta_i = \sin(\theta_i)$  and  $C\theta_i = \cos(\theta_i)$ ; and  $I'_b$  and  $I'_L$  are the moment of inertia of the body and load with respect to the point B, respectively.

$$B = \{m_1 a_{1x} \quad m_1(a_{1y} + g) \quad I_1 \alpha_1 \quad (m_b + m_L)a_{2x} \quad (m_b + m_L)(a_{2y} + g) \\ (I'_b + I'_L)\alpha_2 + (m_b l_b \cos \theta_b + m_L l_L \cos \theta_L)g + m_b l_b(a_{2x} \sin \theta_b - a_{2y} \cos \theta_b) \\ + m_L l_L(a_{2x} \sin \theta_L - a_{2y} \cos \theta_L) \quad m_3 a_{3x} \quad m_3(a_{3y} + g) \\ I_3 \alpha_3 + \frac{m_3 g l_3}{2} \cos(360 - \theta_3) + T_{34} \quad m_4 a_{4x} \quad m_4(a_{4y} + g) \quad I_4 \alpha_4 - T_{34}\}$$

$$X = \{F_1 \quad N_1 \quad F_{12x} \quad F_{12y} \quad F_{23x} \quad F_{23y} \quad F_{34x} \quad F_{34y} \quad F_4 \quad N_4 \quad T_{12} \quad T_{23}\}$$

### References

1. Hirose, S.; Fukushima, E.F.; Damoto, R.; Nakamoto, H. Design of terrain adaptive versatile crawler vehicle HELIOS-VI. In Proceedings of the IEEE International Conference on Intelligent Robots and Systems, Maui, HI, USA, 29 October–3 November 2001; pp. 1540–1545.
2. Lawn, M.J.; Sakai, T.; Kuroiwa, M.; Ishimatsu, T. Development and practical application of a stairclimbing wheelchair in Nagasaki. *Int. J. Hum. Friendly Welf. Robot. Syst.* **2001**, *2*, 33–39.
3. Yu, S.; Wang, T.; Li, X.; Yao, C.; Wang, Z.; Zhi, D. Configuration and tip-over stability analysis for stair-climbing of a new-style wheelchair robot. In Proceedings of the IEEE International Conference on Mechatronics and Automation, ICMA (2010), Xi'an, China, 4–7 August 2010; pp. 1387–1392.
4. Sugahara, Y.; Ohta, A.; Hashimoto, K.; Sunazuka, H.; Kawase, M.; Tanaka, C.; Lim, H.-o.; Takanishi, A. Walking up and down stairs carrying a human by a biped locomotor with parallel mechanism. In Proceedings of the IEEE/RSJ International Conference on Intelligent Robots and Systems, Edmonton, AB, Canada, 2–6 August 2005; pp. 1489–1494.
5. Zhu, Y.; Fei, Y.; Xu, H. Stability analysis of a wheel-track-leg hybrid mobile robot. *J. Intell. Robot. Syst.* **2018**, *91*, 515–528. [\[CrossRef\]](#)
6. Yuan, J.; Hirose, S. Research on leg-wheel hybrid stair-climbing robot, Zero Carrier. In Proceedings of the IEEE International Conference on Robotics and Biomimetics, Shenyang, China, 22–26 August 2004; pp. 654–659.

7. Meghdari, A.; Pishkenari, H.N.; Gaskarimahalle, A.; Mahboobi, S.; Karimi, R. A novel approach for optimal design of a rover mechanism. *J. Intell. Robot. Syst.* **2005**, *44*, 291–312. [CrossRef]
8. Woo, C.-K.; DoChoi, H.; Yoon, S.; Kim, S.H.; Kwak, Y.K. Optimal design of a new wheeled mobile robot based on a kinetic analysis of the stair climbing states. *J. Intell. Robot. Syst.* **2007**, *49*, 325–354. [CrossRef]
9. Bang, Y.-b.; Lee, C.-h.; Yoo, J.-h.; Lee, K.-m.; Kim, I.-s. Two-legged stair-climbing wheelchair and its stair dimension measurement using distance sensors. In Proceedings of the 11th International Conference on Control, Automation and Systems, Gyeonggi-do, Korea, 26–29 October 2011; pp. 1788–1791.
10. Wang, H.; He, L.; Li, Q.; Zhang, W.; Zhang, D.; Xu, P. Research on a kind of leg-wheel stair-climbing wheelchair. In Proceedings of the IEEE International Conference on Mechatronics and Automation, Tianjin, China, 3–6 August 2014; pp. 2101–2105.
11. Zúñiga-Avilés, L.; Pedraza-Ortega, J.; Gorrostieta-Hurtado, E.; Tovar-Arriaga, S.; Ramos-Arreguín, J.; Aceves-Fernández, M.A.; Vargas-Soto, J. Htg-based kinematic modeling for positioning of a multi-articulated wheeled mobile manipulator. *J. Intell. Robot. Syst.* **2014**, *76*, 267–282. [CrossRef]
12. Bruzzone, L.; Fanghella, P. Functional redesign of mantis 2.0, a hybrid leg-wheel robot for surveillance and inspection. *J. Intell. Robot. Syst.* **2016**, *81*, 215–230. [CrossRef]
13. Qiao, G.; Song, G.; Zhang, Y.; Zhang, J.; Li, Z. A wheel-legged robot with active waist joint: Design, analysis, and experimental results. *J. Intell. Robot. Syst.* **2016**, *83*, 485–502. [CrossRef]
14. Stair-Climbing Wheelchair Carrier. 1986. Available online: <https://patents.google.com/patent/CA2204093C/un> (accessed on 30 July 2021).
15. Lawn, M.J.; Ishimatsu, T. Modeling of a stair-climbing wheelchair mechanism with high single-step capability. *IEEE Trans. Neural Syst. Rehabil. Eng.* **2003**, *11*, 323–332. [CrossRef] [PubMed]
16. Liu, J.; Wu, Y.; Guo, J.; Chen, Q. High-Order Sliding Mode-Based Synchronous Control of a Novel Stair-Climbing Wheelchair Robot. *J. Control Sci. Eng.* **2015**, *2015*, 1–16. [CrossRef]
17. Chocoteco, J.; Morales, R.; Feliu, V.; Sanchez, L. Trajectory Planning for a Stair-Climbing Mobility System Using Laser Distance Sensors. *IEEE Syst. J.* **2016**, *10*, 944–956. [CrossRef]
18. Gonzalez, A.; Ottaviano, E.; Ceccarelli, M. On the kinematic functionality of a four-bar based mechanism for guiding wheels in climbing steps and obstacles. *Mech. Mach. Theory* **2009**, *44*, 1507–1523. [CrossRef]
19. Morales, R.; Feliu, V.; González, A. Optimized obstacle avoidance trajectory generation for a reconfigurable staircase climbing wheelchair. *Robot. Auton. Syst.* **2010**, *58*, 97–114. [CrossRef]
20. Morales, R.; Feliu, V.; Gonzalez, A.; Pintado, P. Coordinated motion of a new staircase climbing wheelchair with increased passenger comfort. In Proceedings of the IEEE International Conference on Robotics and Automation, Orlando, FL, USA, 15–19 May 2006; pp. 3995–4001.
21. Morales, R.; Feliu, V.; Gonzalez, A.; Pintado, P. Kinematic Model of a New Staircase Climbing Wheelchair and its Experimental Validation. *Int. J. Robot. Res.* **2006**, *25*, 825–841. [CrossRef]
22. Morales, R.; Gonzalez, A.; Feliu, V.; Pintado, P. Environment adaptation of a new staircase-climbing wheelchair. *Auton. Robot.* **2007**, *23*, 292. [CrossRef]
23. Ghani, N.M.A.; Nasir, A.N.K.; Tokhi, M.O. Optimization of fuzzy logic scaling parameters with spiral dynamic algorithm in controlling a stair climbing wheelchair: Ascending task. In Proceedings of the 19th International Conference on Methods and Models in Automation and Robotics (MMAR), Miedzyzdroje, Poland, 2–5 September 2014; pp. 776–781.
24. Shino, M.; Tomokuni, N.; Murata, G.; Segawa, M. Wheeled inverted pendulum type robotic wheelchair with integrated control of seat slider and rotary link between wheels for climbing stairs. In Proceedings of the IEEE International Workshop on Advanced Robotics and its Social Impacts, Evanston, IL, USA, 11–13 September 2014; pp. 121–126.
25. Chen, C.T.; Pham, H.V. Design and fabrication of a statically stable stair-climbing robotic wheelchair. *Ind. Robot* **2009**, *36*, 562–569. [CrossRef]
26. Sugahara, Y.; Yonezawa, N.; Kosuge, K. A novel stair-climbing wheelchair with transformable wheeled four-bar linkages. In Proceedings of the IEEE/RSJ 2010 International Conference on Intelligent Robots and Systems, Taipei, Taiwan, 18–22 October 2010; pp. 3333–3339.
27. Quaglia, G.; Franco, W.; Oderio, R. Wheelchair.q, a mechanical concept for a stair climbing wheelchair. In Proceedings of the 2009 IEEE International Conference on Robotics and Biomimetics (ROBIO), Guilin, China, 19–23 December 2009; pp. 800–805.
28. Quaglia, G.; Franco, W.; Oderio, R. Wheelchair.q, a motorized wheelchair with stair climbing ability. *Mech. Mach. Theory* **2011**, *46*, 1601–1609. [CrossRef]
29. Quaglia, G.; Maffiodo, D.; Franco, W.; Appendino, S.; Oderio, R. The Epi.q-1 Hybrid Mobile Robot. *Int. J. Robot. Res.* **2009**, *29*, 81–91. [CrossRef]
30. Quaglia, G.; Nisi, M. Design and Construction of a New Version of the EPI.Q UGV for Monitoring and Surveillance Tasks. In Proceedings of the ASME 2015 International Mechanical Engineering Congress and Exposition, Houston, TX, USA, 13–19 November 2015; pp. 1–8.
31. Quaglia, G.; Oderio, R.; Bruzzone, L.; Razzoli, R. A modular approach for a family of ground mobile robots. *Int. J. Adv. Robot. Syst.* **2013**, *10*, 196. [CrossRef]
32. Evolution of Wheelchair.q, a Stair-Climbing Wheelchair. Available online: <https://www.semanticscholar.org/paper/Evolution-of-Wheelchair.q2C-a-Stair-climbing-Quaglia-Franco/394ce9ff2eff245ee7ae711d94a581f5361a5778> (accessed on 18 July 2021).

- 
33. Quaglia, G.; Nisi, M. Design of a Reconfiguration Mechanism for an Electric Stair-Climbing Wheelchair. In Proceedings of the ASME 2014 International Mechanical Engineering Congress and Exposition, Montreal, QC, Canada, 14–21 November 2014; pp. 1–10.
  34. Quaglia, G.; Nisi, M. Design of a self-leveling cam mechanism for a stair climbing wheelchair. *Mech. Mach. Theory* **2017**, *112*, 84–104. [[CrossRef](#)]
  35. Baishya, N.J.; Ogai, H. Wa-chair: A concept for development of economical stair-climbing wheelchair. *IOP Conf. Ser. Mater. Sci. Eng.* **2018**, *307*, 012010. [[CrossRef](#)]
  36. Baishya, N.J.; Ogai, H.; Bhattacharya, B. Design and development of a new active slider crank mechanism based step climbing wheelchair. In Proceedings of the 12th Asian Control Conference (ASCC), Kitakyushu, Japan, 9–12 June 2019; pp. 271–276.